



## Vibrating soap lm: origin of the dissipation

Sébastien Kosgodagan Acharige, Florence Elias, Caroline Derec

► **To cite this version:**

Sébastien Kosgodagan Acharige, Florence Elias, Caroline Derec. Vibrating soap lm: origin of the dissipation. 2014. <hal-00992344>

**HAL Id: hal-00992344**

**<https://hal.archives-ouvertes.fr/hal-00992344>**

Submitted on 16 May 2014

**HAL** is a multi-disciplinary open access archive for the deposit and dissemination of scientific research documents, whether they are published or not. The documents may come from teaching and research institutions in France or abroad, or from public or private research centers.

L'archive ouverte pluridisciplinaire **HAL**, est destinée au dépôt et à la diffusion de documents scientifiques de niveau recherche, publiés ou non, émanant des établissements d'enseignement et de recherche français ou étrangers, des laboratoires publics ou privés.

# Vibrating soap film: origin of the dissipation

S. Kosgodagan Acharige<sup>1</sup>, F. Elias<sup>1,2</sup>, C. Derec<sup>1</sup>

<sup>1</sup> Laboratoire Matière et Systèmes Complexes (MSC), Université Paris-Diderot, CNRS UMR 7057, Paris, France

<sup>2</sup> Sorbonne Universités, UPMC Université Paris 6, UFR 925, Paris, France

**Abstract.** We investigate the complex dispersion relation of a transverse antisymmetric wave on a horizontal soap film. Experimentally, the complex wave number  $k$  at a fixed forcing frequency is determined by measuring the vibrating amplitude of the soap film: the wavelength (linked to the real part of  $k$ ) is determined by the spatial variation of the amplitude; the decay length (linked to the imaginary part of  $k$ ) is determined by analyzing the resonance curves of the vibrating wave as a function of the frequency. Theoretically, we compute the complex dispersion relation taking into account the physical properties of the bulk liquid and gas phase, and of the gas-liquid interfaces. The comparison between the computation (developed to the leading order in our experimental conditions) and the experimental results confirms that the phase velocity is fixed by the interplay between surface tension, and liquid and air inertia, as reported in previous studies. Moreover, we show that the attenuation of the transverse antisymmetric wave originates from the viscous dissipation in the gas phase surrounding the liquid film. This result is an important step to understand the propagation of an acoustic wave in a liquid foam, in a bottom-up approach.

## 1. Introduction

Although solid foams are commonly used as acoustic dampers [1, 2], little is known about the acoustic properties of liquid foams, which are dispersions of gas bubbles in a liquid matrix stabilized by surfactants. Recent studies report measurements of the velocity and attenuation of sound in liquid foams: several regimes of propagation have been identified as a function of the frequency, as well as acoustic resonances [3, 4, 5, 6]. Various sources of attenuation have been invoked to account for the observations, which depend on the bulk properties of the gas and liquid phase (compressibility, density and viscosity), on the interfacial properties of the liquid-gas interfaces and on the local structure of the foam. The foam liquid skeleton is made of thin membranes (soap films), Plateau borders (which contain most of the liquid of the foam) at the junction between soap films, and vertices at the junction between Plateau borders [7]: the vibration motion of all those constitutive elements is mechanically coupled during the acoustic wave propagation. Understanding the vibration of those individual elements is fundamental to model their coupling and therefore the acoustic propagation in liquid foams.

In this article, we are interested in the vibration motion of one of those elements: an individual soap film isolated on a rigid frame. We investigate the response of the film to a transverse vibration by measuring and modeling the dispersion relation and the attenuation of the wave propagating on the film.

Various linear models of the dispersion relation of a transverse vibration on horizontal soap films exist in the literature [8, 9, 10]. They differ by the ingredients taken into account, amongst the physical characteristics of the bulk liquid and gas phases (volume mass and viscosity) and of the liquid-gas interface (surface tension and interfacial visco-elasticity). They predict two oscillation modes, a squeezing or symmetric mode (where both interfaces vibrate symmetrically with respect to the middle plane of the film), and an antisymmetric or bending mode (where the interfaces vibrate in phase). Due to the strong viscous friction associated with the symmetric mode, the most commonly observed vibration mode is the bending mode. An experimental measurement of the dispersion relation of the bending mode, reported in ref. [11], shows that the elastic restoring force is due to the surface tension, whereas inertia comes from the inertia of the liquid in the soap film and from the inertia of the air, which is dominant at low frequency. The attenuation of the wave is very low and has not been measured to our knowledge. At large vibrating amplitude, non-linear behaviors of vibrated soap films have also been observed and studied. They concern the generation of vortices within the plane of the film [11], the self-adaptation of the local thickness of the soap film to the vibration amplitude [12], the formation of a liquid bulge in the middle of the film, and the soap film bursting at high forcing amplitude [13].

In this article, we investigate the complex dispersion relation of the bending mode of a soap film. Whereas the real part of the dispersion relation confirms the variation of the wavelength versus the frequency already reported in the literature [8, 14, 11], the imaginary part enables us to determine the attenuation of the vibrating wave. We report here for the first time a theoretical modeling of the attenuation, as well as an experimental determination of the attenuation length. This determination is based on the measurement of the amplitude of a standing transverse wave on the film around the geometrical resonances, in the frequency range 200-2000 Hz. The film is vibrated with a low forcing amplitude so that non-linear effects are not observed. The comparison between the experimental results and the analytical model developed to the leading order shows that, in our experimental conditions, the attenuation of the transverse wave originates from the viscous dissipation in the surrounding air. This result can be compared with the case of microscale mechanical resonator where the viscous damping of the air may be an important limiting factor for mass detection [15].

The article is organized as follows. The experimental setup and methods of analysis are described in section 2. In section 3, we present the measurements of the real part of the dispersion relation, and of the soap film amplitude which shows resonant modes of the standing vibrating wave. The theoretical complex dispersion relation is derived in section 4. In section 5, the complex dispersion relation is simplified to the leading order in our experimental conditions. It is divided into its real part and its imaginary

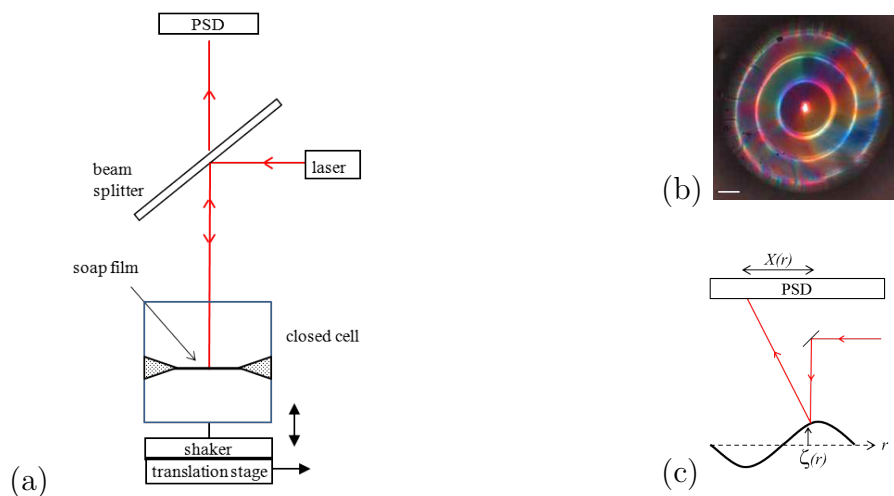


**Figure 1.** (a) Experimental setup (see text); (b) image of a vibrating soap film (obtained by illuminating the film with a parallel white light and using a CCD camera placed above the film): the bright rings correspond to the antinodes of the standing vibrating wave (frequency  $f = 1196$  Hz; film thickness  $e = 1.3 \mu\text{m}$ , the soap film is formed with TTAB and glycerol in water – no LOH); (c) principle of the measurement of the deformation of the film and notations: the film is represented at a given time  $t$ ; the deflection  $X$  of the laser beam is linked to the local slope of the film  $\partial\zeta/\partial r$ . (For the sake of clarity, the length scales are not respected.)

part, which are both separately compared to the experimental results. The theory and the experimental data agree very well, although some additional parameters have to be added to the model, probably due to the presence of the meniscus linking the film to its rigid support. Concluding remarks are given in section 6, and the results are discussed: they are compared to the propagation of a transverse wave on a monolayer, and outlooks of this work are suggested in terms of investigating the coupling between the soap film and the meniscus dynamics.

## 2. Materials and methods

### 2.1. Experimental setup

The liquid films are made from a solution of deionized water and an cationic surfactant TTAB (tetradecyltrimethylammonium bromide) with a concentration of 2.8 g/L. Glycerol (10%wt) and dodecanol (0.04%wt) are added to increase the film stability, extending the duration of the film from a few minutes to a few days. The surface tension  $\gamma$  and interfacial viscoelastic complex modulus  $\epsilon = \epsilon' + \epsilon''$  are measured using an oscillating bubble tensiometer:  $\gamma = 22.5$  mN/m,  $\epsilon' = 5$  mN/m,  $\epsilon'' = 25$  mN/m at 0.1 Hz. The mass density of the liquid phase is  $\rho = 1.0 \cdot 10^3$  kg.m<sup>-3</sup> and its dynamic viscosity is  $\eta \simeq 1.3 \cdot 10^{-3}$  Pa.s.

The soap film is formed on a rigid porous glass plate having a circular bevelled hole in the middle (hole diameter 16.2 mm): the porous plate is saturated with the

soap solution, and the film is stretched from the border of the hole using a Teflon slide. The porous plate is clamped horizontally in the middle of a closed cell (internal height larger than twice the soap film diameter). Just after the soap film is formed, the cell is mounted on a drill where the film is centrifuged for a few minutes, as in ref. [16], until it becomes a homogeneous black film (thickness  $e \simeq 0.01$  to  $0.1 \mu\text{m}$ ). Then, the cell is placed on a shaker that creates a vertical displacement at a given frequency  $f$ , the film being horizontal (Fig. 1a). A centripetal circular transverse wave is created on the film from the borders; the wave is totally reflected at the centre of the film, and a resulting standing wave takes place on the soap film at the forcing frequency (Fig. 1b). Depending on  $f$ , resonances are then observed for some defined ratio of the wavelength versus the soap film diameter.

The amplitude of the transverse wave is determined using a laser beam, set at normal incidence when the film is at rest: the beam, reflected by the soap film, is deflected when the film is deformed. The horizontal deflection  $X$  is recorded using a position sensitive detector (PSD) placed above the film.  $X$  is related to the value of the local slope of the film:

$$X(r, t) = 2D \frac{\partial \zeta}{\partial r}(r, t) \quad (1)$$

where  $\zeta(r, t)$  is the vertical displacement of the circular soap film at a distance  $r$  from the centre at time  $t$  and  $D$  is the distance between the soap film and the PSD (Fig. 1c). Eq. (1) is valid for  $\zeta \ll D$  and for  $\zeta \ll \lambda$  where  $\lambda$  is the wavelength of the antisymmetric vibration. The PSD is connected to a lock-in amplifier which measures the deflection  $X$  at the forcing frequency.

The shaker is placed on a motorized translation stage to scan the local slope along a diameter of the vibrating film.

The electric shaker vibrates with a constant acceleration, therefore the amplitude of the forcing decreases with the forcing frequency like  $1/f^2$ . The amplitude  $\mathcal{A}_{cell}$  of the cell placed on the shaker is determined independently using an accelerometer in order to calibrate the setup. We notice that the cell fixed on the shaker introduces an additional resonance around 1200 Hz.

## 2.2. Data analysis

In the large wavelength limit (wavelength large compared to the vertical displacement and to the thickness of the film), the standing wave having a cylindrical symmetry writes

$$\zeta(r, t) = \mathcal{A}_0 J_0(kr) e^{i(\omega t + \phi_0)} \quad (2)$$

where  $\mathcal{A}_0$  is the displacement amplitude at  $r = 0$ ,  $J_0$  is the Bessel function of the first kind and of zero order,  $\omega = 2\pi f$  is the angular frequency,  $k = k' + ik''$  is the complex wave number and  $\phi_0$  is the phase at  $r = 0$  and  $t = 0$ . In those conditions, Eq. (1) becomes

$$X(r, t) = -2D\mathcal{A}_0 k J_1(kr) e^{i(\omega t + \phi_0)} = |X| e^{i\psi} e^{i\omega t} \quad (3)$$

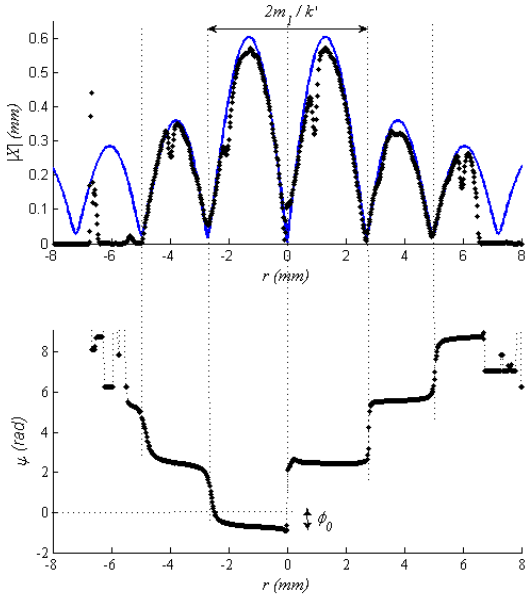


**Figure 2.** Amplitude of the deflection of the laser beam measured at  $f = 1140$  Hz: modulus  $|X|$  and argument  $\psi$  of  $X$  as a function of the position  $r$  from the centre of the film (diamonds). In the top graph, the solid line is the best fit of the data using Eq. (3) with  $k = k' + ik''$ . One finds  $k' = 1410 \text{ m}^{-1}$  and  $\mathcal{A}_0 = 2.2 \text{ }\mu\text{m}$ . The vertical dotted lines highlight the method used to determine the value of  $k'$  (example here with  $m_1 = 3.83$  the first zero of the Bessel function  $J_1(k'r)$ ). The bottom graph shows the determination of the phase shift  $\phi_0$  around  $r = 0$ .

The modulus  $|X|$  and the argument  $\psi$  of the laser beam deflection are measured, at the angular frequency  $\omega$ , thanks to the lock-in amplifier.

We write a boundary condition:

$$\zeta(R, t) = \mathcal{A}_b e^{i(\omega t + \phi_b)}. \quad (4)$$

where  $\mathcal{A}_b$  and  $\phi_b$  are respectively the amplitude and phase of the displacement at a distance  $R$  from the centre of symmetry. Combined with Eq. (2), this gives:

$$\begin{cases} \mathcal{A}_0 = \mathcal{A}_b / |J_0(kR)| \\ \phi_0 = \phi_b - \arg(J_0(kR)) \end{cases} \quad (5)$$

Eq. (5) predicts resonances of the soap film transverse vibration when  $|J_0(kR)|$  is minimum. Let us note that the minimal value of  $|J_0(kR)|$  does not reach zero due to the imaginary part  $k''$  of the wave vector. Moreover, the variation of  $\mathcal{A}_0$  and  $\phi_0$  around the resonance frequencies strongly depends on the value of  $k''$ . Therefore, the measurement of the transverse wave attenuation  $k''$  is based on the analysis of the shape of the resonance curves, as explained below.

### 3. Measurements

Fig. 2 shows the measurements of the modulus and the argument of the amplitude of the laser beam deflection  $X(r)$  at a given frequency.  $|X(r)|$  is compared to eq. (3) using  $k'$ ,  $k''$  and  $\mathcal{A}_0$  as free parameters. The best fit gives the measurement of  $k'$  and  $\mathcal{A}_0$ . However, the fit poorly depends on the value of  $k''$ , which cannot reasonably be determined with this method. The phase shift  $\phi_0$  is determined graphically using the plot of  $\psi(r)$  as shown in Fig. 2.

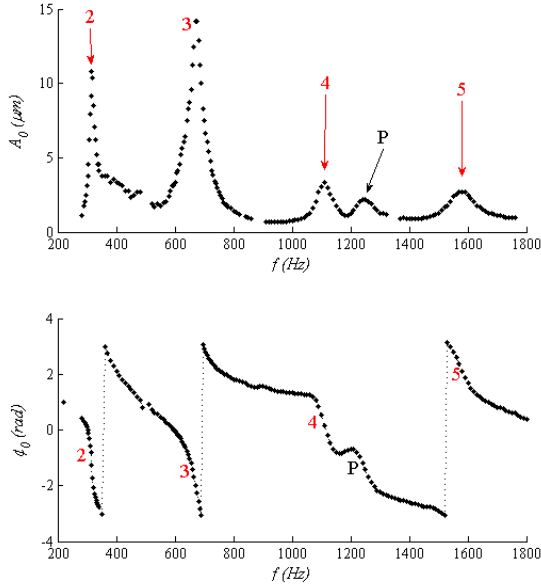


**Figure 3.** Amplitude  $\mathcal{A}_0$  and phase shift  $\phi_0$  in the centre of the film as a function of the frequency  $f$ , measured as described in Fig. 2, showing the resonances of the transverse standing wave of the film.

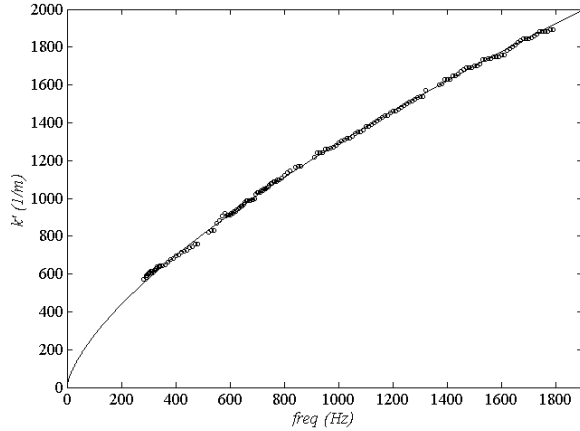


**Figure 4.** Real part of the wave vector  $k'$  as a function of the frequency  $f$ : experimental measurements obtained as described in Fig.2 (circles) and best fit using Eq. (17) with the thickness  $e$  of the soap film as a fitting parameter (here  $e = 83$  nm).

The parameters  $k'$ ,  $\mathcal{A}_0$  and  $\phi_0$  are then plotted as a function of the frequency (Figs. 3 and 4). Five resonances are visible on Fig. 3: one of them, around 1240 Hz and denoted by ‘P’, is identified as a resonance of the setup. The four other resonances correspond to resonances of the soap film: the analysis of the profiles  $|X(r)|$  shows that they correspond to modes  $n = 2, 3, 4$  and  $5$ , having  $(2n - 1)$  antinodes along the diameter of the film. Those modes are expected considering the axisymmetric geometry of the vibrating film with an antinode in the centre according to Eq. (2). Surprisingly, the fundamental mode ( $n = 1$ ) could not be observed, the vibrating amplitude being too small to be detected for frequencies lower than 280 Hz.

Fig. 4 shows the variation of  $k'$ , extracted from the determination of  $X(r)$ , as a function of the frequency: one notices that the wave propagation is dispersive, with an increasing phase velocity  $\omega/k'$  versus  $f$ .

#### 4. Theoretical dispersion relation

In this section we compute the complex dispersion relation of the transverse wave on the horizontal soap film. We consider a liquid film of constant thickness  $e = 2h$ . The liquid has a viscosity  $\eta$  and a constant mass density  $\rho$ . The wavelength is assumed to be large compared to  $e$  and to the amplitude  $\zeta$  of the vertical displacement. For simplicity, we consider here a two-dimensional problem: the film at rest is along the  $x$  axis; the transverse wave, a deformation along the  $z$  axis, propagates in the  $x$  direction. In other words, the problem is infinite in the perpendicular  $y$  direction. With the parameters cited above, and also taking into account the interfacial visco-elastic modulus  $\epsilon$  and the inertia of the air  $\rho_a$ , we have checked that the same calculation performed in a 3D geometry with an axial symmetry leads to the same dispersion relation.

Moreover, we develop here the calculations also taking into account the viscosity of the air,  $\eta_a$ . To our knowledge, it has been considered theoretically only by Joosten [8], in the MHz regime and in the limit of incompressible interfaces ( $\epsilon \rightarrow \infty$ ). The calculation presented here extends this approach to other regimes, in particular to the kHz regime and the case of a finite  $\epsilon$  corresponding to our experimental conditions.

##### 4.1. Velocity and pressure fields for an antisymmetric vibration

The velocity field  $\vec{v}$  of a liquid volume element obeys the incompressibility condition and the Navier-Stokes equation:

$$\begin{cases} \operatorname{div}(\vec{v}) = 0 \\ \rho \partial_t \vec{v} = -\vec{\nabla} P + \eta \overline{\Delta} \vec{v} + \rho \vec{g} \end{cases} \quad (6)$$

where  $P$  is the local pressure and  $\vec{g}$  is the gravitational acceleration.  $\partial_t$  stands for the partial derivation with respect to time  $t$ . The nonlinear inertial term in the Navier-Stokes equation has been neglected in the long wavelength limit.

The velocity field can be written as a combination of a potential flow and a rotational flow:  $\vec{v}(x, z, t) = -\overrightarrow{\operatorname{grad}}\Phi + \overrightarrow{\operatorname{rot}}\vec{\Psi}$ , where  $\Phi(x, z, t)$  is the potential function and  $\vec{\Psi} = \Psi(x, z, t)\vec{e}_y$  is the vorticity function,  $\vec{e}_y$  being a unit vector in the  $y$  direction. Therefore

$$\begin{cases} \Delta\Phi = 0 \\ -\rho \partial_t \Phi + (P - P_0) - \rho g(h - z) = 0 \\ -\rho \partial_t \Psi + \eta \Delta \Psi = 0 \end{cases} \quad (7)$$

where  $P_0$  is the pressure at rest at  $z = h$ . For an antisymmetric solution,  $\Phi(x, -z, t) = -\Phi(x, z, t)$  and  $\Psi(x, -z, t) = \Psi(x, z, t)$  (the origin of the  $z$  axis is chosen in the plane of symmetry of the film at rest). The solutions corresponding to an oscillation at the angular frequency  $\omega$ , propagating in the  $x$  direction write

$$\begin{cases} \Phi(x, z, t) = A \sinh(kz) e^{i(\omega t - kx)} \\ \Psi(x, z, t) = B \cosh(mz) e^{i(\omega t - kx)} \end{cases} \quad (8)$$

where  $k = k' + ik''$  is the complex wave number (note that here a damped oscillation corresponds to a negative  $k''$ ), and  $m^2 = k^2 + i\rho\omega/\eta$ .  $A$  and  $B$  are two integration constants. We then obtain

$$\begin{cases} v_x(x, z, t) = (ikA \sinh(kz) - mB \sinh(mz)) e^{i(\omega t - kx)} \\ v_z(x, z, t) = (-kA \cosh(kz) - ikB \cosh(mz)) e^{i(\omega t - kx)} \end{cases} \quad (9)$$

and, using Eq. (7),

$$P(x, z, t) = P_0 + \rho g(h - z) + i\rho\omega A \sinh(kz) e^{i(\omega t - kx)} \quad (10)$$

The motion of the air under and above the film must also be considered. The velocity field in the air  $\vec{v}_a$  is calculated using the same approach as above. We write  $\vec{v}_a(x, z, t) = -\overrightarrow{\text{grad}}\Phi_a + \overrightarrow{\text{rot}}\vec{\Psi}_a$  with  $\vec{\Psi}_a = \Psi_a \vec{e}_y$ . Since the propagation velocity of the perturbation is small compared to the sound velocity in the air, the air is assumed to be incompressible. Therefore

$$\begin{cases} \text{div}(\vec{v}_a) = 0 \\ \rho_a \partial_t \vec{v}_a = -\vec{\nabla} P_a + \eta_a \overrightarrow{\Delta} \vec{v}_a + \rho_a \vec{g} \end{cases} \quad (11)$$

where  $\rho_a$  and  $\eta_a$  are respectively the mass density and the dynamic viscosity of the air. Using the same argument as previously (Eq. (7)) and taking into account the boundary conditions  $\Phi_a(x, z, t), \Psi_a(x, z, t) \rightarrow 0$  when  $z \rightarrow \infty$ , the solutions are, for  $z \geq Z_1$ , where  $Z_1$  is the position of the upper interface of the film:

$$\begin{cases} \Phi_a(x, z, t) = C \exp(-kz) e^{i(\omega t - kx)} \\ \Psi_a(x, z, t) = D \exp(-m_a z) e^{i(\omega t - kx)} \end{cases} \quad (12)$$

with  $m_a^2 = k^2 + i\rho_a\omega/\eta_a$ , and  $C$  and  $D$  two integration constants. The velocity field and the pressure field in the air can then be deduced from Eq. (12).

#### 4.2. Continuity of the velocity and of the stress at the interface

We now consider the liquid-air interfaces. The continuity of the tangential and normal stresses at the upper interface ( $Z_1 \simeq h$ ) writes:

$$\begin{cases} -\eta (\partial_z v_x + \partial_x v_z)_h + \eta_a (\partial_z v_{ax} + \partial_x v_{az})_h + \epsilon \partial_{xx} \xi = 0 \\ (P - P_a)_h - 2\eta (\partial_z v_z)_h + 2\eta_a (\partial_z v_{az})_h + \gamma \partial_{xx} \zeta = 0 \end{cases} \quad (13)$$

where  $\xi$  and  $\zeta$  are the displacements respectively along  $x$  and  $z$  of the upper interface  $Z_1$ , and  $\epsilon = S d\gamma/dS$  is the viscoelastic modulus,  $S$  being the interfacial infinitesimal area. In our case the surface is one dimensional, therefore  $\epsilon = d\gamma/dx\xi$ . In the first equation, the tangential viscous forces in the liquid and in the air are balanced by the interfacial viscoelastic stress in the plane of the interface. The second equation balances the pressure jump at the interface with the viscous normal forces in the liquid and in the air, and the normal force coming from the interfacial curvature.

In the long wavelength limit,  $\xi$  et  $\zeta$  are given by

$$\begin{cases} \partial_t \xi \simeq v_x(Z_1) \simeq v_x(h) \\ \partial_t \zeta \simeq v_z(Z_1) \simeq v_z(h) \end{cases}$$

Therefore

$$\begin{cases} \xi(x, t) = \omega^{-1} [kA \sinh(kh) + imB \sinh(mh)] e^{i(\omega t - kx)} \\ \zeta(x, t) = \omega^{-1} [ikA \cosh(kh) - kB \cosh(mh)] e^{i(\omega t - kx)} \end{cases} \quad (14)$$

Moreover the continuity of the  $x$  and  $z$  components of the velocities  $\vec{v}$  and  $\vec{v}_a$  at the interface leads to an expression of  $v_{ax}$ ,  $v_{az}$  and  $P_a$  as a function of the constants  $A$  and  $B$  (instead of  $C$  and  $D$ ).

#### 4.3. Dispersion relation

Eqs. (13) couple the velocity fields and the pressure fields in the air and in the liquid. Using the expressions determined previously for those fields, they result in a system of two equations with two unknowns,  $A$  and  $B$ . The discriminant has to be equal to zero. To the first order in  $kh$  and  $mh$  (long wavelength limit), this gives the dispersion relation:

$$\frac{\omega^2}{k^2} \left( \rho h + \frac{\rho_a}{k} \frac{m_a}{m_a - k} \right) = \gamma + \frac{\eta \omega}{\eta \omega - i \epsilon k^2 h} \left[ \epsilon (kh)^2 + E \right] \quad (15)$$

with

$$\begin{aligned} E = & \gamma \frac{\eta_a}{\eta} (k + m_a) h + \frac{\rho_a \omega^2 h}{k(m_a - k)} \left( 1 - \frac{\eta_a}{\eta} \frac{k^2 + m_a^2}{k^2} \right) \\ & - i \eta_a \omega h \left[ \left( -3 + 2 \frac{\eta_a}{\eta} \right) + \frac{m_a}{k} \left( 1 - 2 \frac{\eta_a}{\eta} \right) - \frac{m^2}{k^2} (k + m_a) h \right] \end{aligned}$$

## 5. Comparison between theory and experimental results

In our experimental conditions, Eq. (15) can be simplified. It is developed to the first order in  $k''/k'$ . Furthermore,  $\eta_a \simeq 2.10^{-5}$  Pa.s is neglected compared to  $\eta$ . We use the values of the physical parameters given in section 2.1,  $\rho_a \simeq 1 \text{ kg.m}^{-3}$  and  $e \sim 1 \text{ } \mu\text{m}$  or less. Using the relation  $\eta_a k'^2 / (\rho_a \omega) \ll 1$  and considering the case  $|\epsilon| h \leq 10^{-7} \text{ N}$  so that  $|\epsilon k^2 h| / (\eta \omega) \ll 1$ , eq. (15) is simplified to the leading order and divided into a real part and an imaginary part.

### 5.1. Real part of the dispersion relation

Taking into account the orders of magnitude corresponding to our experimental conditions and range of frequencies, the real part of the dispersion relation is simplified in two steps. First we keep the leading order for each physical ingredient, in particular  $\eta_a$  and  $\epsilon$ , and we get the following equation :

$$\frac{\omega^2}{k'^2} \left( \rho h + \frac{\rho_a}{k'} + \rho_a \sqrt{\frac{\eta_a}{2 \rho_a \omega}} \right) \simeq \gamma + \theta (k' h)^2 \epsilon' \quad (16)$$

with  $\theta$  a multiplying factor of the order of 1.

The phase velocity  $\omega/k'$  is given by the ratio between the restoring force (terms in the right-hand side of the equation) and the inertia (terms in brackets in the left-hand

side). The main effect of the interfacial viscoelasticity  $\epsilon$  is thus a small correction to the restoring force, whereas the main effect of the viscosity of the air is a slight increase in the inertia.

These two corrections are actually negligible in our experimental conditions and we get finally the real part of the simplified dispersion relation :

$$\frac{\omega^2}{k'^2} \left( \rho e + 2 \frac{\rho_a}{k'} \right) \simeq 2\gamma \quad (17)$$

The phase velocity is thus essentially given by the ratio between the surface tension of the film, which acts as a restoring force, and the inertia. The air is displaced on a vertical distance of the order of the wavelength, therefore the inertia of the air cannot be neglected in comparison with the inertia of the liquid in the film.

Eq. (17) has already been predicted in previous studies [8, 14, 11]. Our calculation shows that this expression is robust even if parameters such as the interfacial viscoelasticity and viscosities of the liquid and the air are taken into account: they have a negligible role in our experimental conditions. Note that Eq. (17) is still valid if  $|\epsilon|$  is as large as 1 N/m, since the viscoelastic term is always multiplied by  $(kh)^2$  (see Eq. (15)) which is of order  $10^{-6}$ .

Fig. 4 shows a comparison of Eq. (17) with the experimental measurements of  $k'$  versus  $f = \omega/(2\pi)$ , using  $e$  as a fitting parameter: the agreement is excellent. Let us notice that the fit poorly depends on  $e$ : in our experimental conditions,  $e$  is smaller than 100 nm and the inertia of the air is actually larger than the inertia of the liquid. Would  $e$  vary by 30 percent, the adjustment would still be satisfying.

## 5.2. Imaginary part

The imaginary part of the dispersion relation becomes, when keeping only the leading term describing the effects of the viscosity  $\eta_a$  and of the interfacial viscoelasticity  $\epsilon$  :

$$\frac{\omega^2}{k'^2} \left( \frac{-k''}{k'} \left( \rho e + 3 \frac{\rho_a}{k'} \right) - \rho_a \sqrt{\frac{\eta_a}{2\rho_a\omega}} \right) \simeq \beta (k'h)^2 \epsilon'' \quad (18)$$

where  $\beta$  is a multiplying factor of the order of 1.

The contribution of the surface viscosity  $\epsilon''$  to the attenuation is very small compared to the contribution of the viscosity of the air, and the simplified imaginary part of the dispersion relation is finally :

$$\frac{-k''}{k'} \left( \rho e + 3 \frac{\rho_a}{k'} \right) \simeq \rho_a \sqrt{\frac{\eta_a}{2\rho_a\omega}} \quad (19)$$

Eq. (19) predicts that the attenuation of the transverse wave is mainly determined by the air viscosity. The quantity  $\sqrt{\eta_a/(2\rho_a\omega)} \simeq 50 \mu\text{m}$  appears as the typical distance over which the dissipation in air takes place. The effects of the fluid viscosity and of the interfacial viscoelasticity can be neglected.

### 5.3. Measurement of $k''$ and comparison with the theory

The experimental measurement of  $k''$  is based on the analysis of the shape of the resonances presented in Fig. 3:  $k''$  corresponds to the best fit of the experimental data using Eq. (5), performed as follows. The measurements of  $\mathcal{A}_0$  and  $\phi_0$  are plotted as a function of  $k'$  using Eq. (17) to convert the (angular) frequency in terms of the real part  $k'$  of the wave vector. The amplitude  $\mathcal{A}_0$  is divided by the vibration amplitude of the cell  $\mathcal{A}_{cell}$ , measured independently at the same frequency. The results are shown in Fig. 5 around one resonance.  $[\mathcal{A}_0/\mathcal{A}_{cell}](k')$  and  $\phi_0(k')$  are then fitted using the following expressions, extracted from Eq. (5):

$$\begin{cases} \mathcal{A}_0/\mathcal{A}_{cell} = \alpha/|J_0(kR)| \\ \phi_0 = \phi_b - \arg(J_0(kR)) \end{cases} \quad (20)$$

The parameters  $R$ ,  $\alpha = \mathcal{A}_b/\mathcal{A}_{cell}$  and  $k''$  are three fitting parameters for the amplitude  $\mathcal{A}_0/\mathcal{A}_{cell}$  around a resonance, which determine respectively the frequency, the amplitude and the width of the resonance peak.  $R$ ,  $\phi_b$  and  $k''$  are also three fitting parameters for the phase  $\phi_0$ . The results of the fits are reported in table 1. The fact that  $\alpha \neq 1$  and  $\phi_b \neq 0$  suggests that the meniscus between the rigid support and the soap film could play a role by attenuating or amplifying the forcing amplitude transmitted from the support to the film, and by introducing a phase difference between the controlled forcing and the border of the film. Moreover the coupling between the response of the meniscus and the response of the soap film could also be responsible for the fact that the position  $R$  of the minimum of  $|J_0(kR)|$  does not correspond exactly to the radius of the support, equal to 8.1 mm. Thus the parameters  $R$ ,  $\alpha$  and  $\phi_b$  are linked to the boundary conditions, as if an effective forcing of amplitude  $\alpha \times \mathcal{A}_{cell}$  and phase  $\phi_b$  would be applied to the soap film at  $r = R$ . On the other hand the parameter  $k''$  is associated to the intrinsic attenuation of the wave on the soap film.

The measurements of  $k''$  extracted from the fits are plotted in Fig. 6 as a function of the frequency of the corresponding mode. The data are compared to the theoretical modeling of  $k''(f)$  (Eq. (17) and (19)) represented on the same graph without any fitting parameter. The agreement between the theory and the measurements is very good.

**Table 1.** Parameters obtained from the best fits of the data using Eq. (20) for a soap film of thickness  $e \simeq 80$  nm (see Fig. 5 for the example of the mode  $n = 5$ ).

	mode 2	mode 3	mode 4	mode 5
$k''$ ( $\text{m}^{-1}$ )	$8 \pm 5$	$15 \pm 5$	$22 \pm 5$	$31 \pm 5$
$R$ (mm)	$9.3 \pm 0.1$	$8.8 \pm 0.1$	$8.5 \pm 0.1$	$8.5 \pm 0.1$
$\alpha$	$0.9 \pm 0.2$	$9 \pm 1$	$6 \pm 0.5$	$15 \pm 1$
$\phi_b$ ( $[\pi]$ )	$0.4 \pm 0.1$	$-0.5 \pm 0.1$	$-1.3 \pm 0.1$	$+0.7 \pm 0.1$

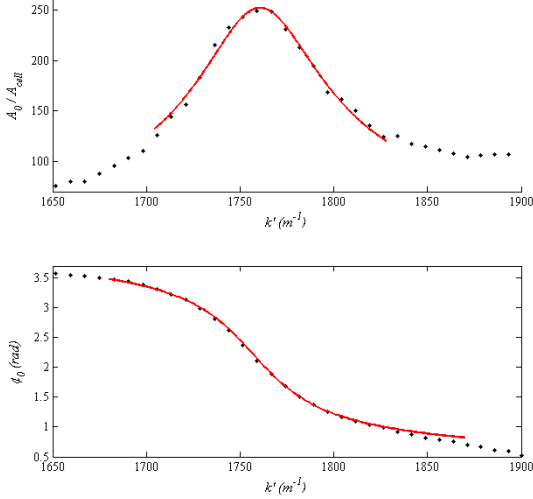


**Figure 5.** Diamonds: amplitude and phase  $\phi_0$  of the standing wave at  $r = 0$ , for the resonant mode  $n = 5$  (see Fig. 3). The amplitude is rescaled by the amplitude of vibration of the experimental cell. Solid lines: fits of the data using Eq. (20) with 3 fitting parameters (see text).

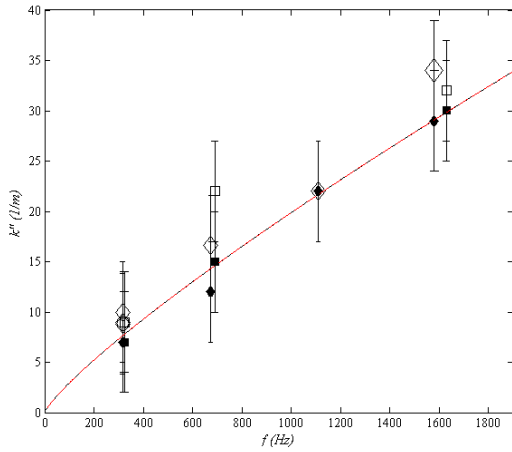


**Figure 6.**  $k''$  as a function of the frequency  $f$  of the resonant modes. The experimental data are extracted from the fits of the amplitude (empty symbols) and of the phase (full symbols) using Eq. (20), for two films of thickness  $e \simeq 60$  nm (squares) and  $e \simeq 80$  nm (diamonds). The solid line corresponds to the model Eq. (17) and (19) without any fitting parameters (the curves for both thicknesses are superimposed).

## 6. Discussion and Conclusion

We have measured the attenuation of a transverse antisymmetric wave on a thin soap film. Since the attenuation is very small (we find  $1/k'' = 3$  to  $14$  cm – larger than the radius of the film – depending on the forcing frequency), its determination is based on the analysis of the width of the resonant curves (amplitude and phase in the centre of the film as a function of the frequency), which strongly depends on the imaginary part  $k''$  of the wave number. The amplitude and phase of the vibrating film were determined by measuring the deflection of a laser beam reflected by the film, at the forcing frequency.

Using the same approach as in refs. [8, 9, 10], we have computed the complex dispersion relation of the antisymmetric waves in the long wavelength limit. We have obtained analytical expressions for the real part and the imaginary part of the dispersion relation, simplified to the leading order in our experimental conditions. The real part (variation of the wavelength with the frequency) agrees with our measurements, taking the film thickness  $e$  as a fitting parameter like in ref. [11]. Concerning the imaginary

part, the very good agreement between the theory and the measurements evidences that, in our experimental conditions, the dominant source of attenuation of the antisymmetric wave on a soap film is the dissipation by viscous friction in the air. This is the main result of this article.

This behavior is very different from the propagation of a transverse wave in a surfactant monolayer at the surface of the liquid solution [17]. In this system, the wave attenuation depends mainly on the rheological properties of the liquid phase and of the liquid-air interface. The measurement of the attenuation of the capillary wave is actually used as a standard technique to determine the surface dilational viscoelastic modulus of the monolayer [18]. Theoretically, the interfacial viscoelasticity acts as a tangential stress which balances, at the interface, the viscous shear stresses in the liquid and in the air (see first line of Eq. (13)). This 2D viscoelastic stress depends on the local displacement  $\xi$  in the plane of the interface. In a vibrating soap film, because of the liquid incompressibility and of the symmetry of the wave,  $\xi$  is of the order of the perpendicular displacement  $\zeta$  of the interface multiplied by  $(k'e)$  (see Eq. (14) in the long wavelength limit), that is,  $\xi \sim 10^{-3}\zeta$ . By contrast,  $\xi \sim \zeta$  in the case of the monolayers. For the same value of the 2D viscoelastic modulus  $\epsilon$ , the tangential 2D viscoelastic stress at the interface of a soap film is therefore three orders of magnitude smaller than the tangential 2D viscoelastic stress at the surface of a monolayer. As a consequence, the viscoelastic interfacial modulus plays no role on the wave attenuation as long as it is smaller than 1 N/m.

A peculiar behavior of some fitting parameters of the model appears in the analysis of the resonances: first, the distance  $R$  of the effective forcing from the centre of the film is slightly larger than the radius of the rigid frame supporting the film; second, the effective forcing amplitude given by the fit is smaller or larger (depending on the frequency) than the vibrating amplitude of the support; third, an additional phase shift between the forcing and the response of the film is observed, which depends on the frequency. All those parameters are linked to the boundary conditions of the soap film. They might reveal a complex behavior of the liquid meniscus that separates the soap film from its support: we interpret the observed shifts in  $R$  and the soap film amplitude and phase of the effective forcing as an effect of the coupling between the soap film and the meniscus. The relative motion between the film and the meniscus could also be responsible for the large attenuation of the transverse wave at low frequency [19]. Further studies will use this experimental setup to investigate this dynamical coupling between the meniscus and the soap film, which is central to understand the acoustic propagation in liquid foams [6].

**Acknowledgements:** The authors thank Valentin Leroy and Benjamin Dollet for fruitful discussions. This work has been supported from the french Agence Nationale de la Recherche (ANR-11-BS09-001).

- [1] K. Attenborough, *Physics Reports*, 1982, **82**, 179.
- [2] J. Allard, N. Atalla, *Propagation of sound in porous media*, Wiley, 2009.
- [3] I. Ben Salem, R.-M. Guillermic, C. Sample, V. Leroy, A. Saint-Jalmes, B. Dollet, *Soft Matter*, 2013, **9**, 1194.
- [4] J. Pierre, F. Elias, V. Leroy, *Ultrasonics*, 2013, **53**, 622.
- [5] J. Pierre, R.-M. Guillermic, F. Elias, W. Drenckhan, V. Leroy, *Eur. Phys. J. E.*, 2013, **36**, 113.
- [6] J. Pierre, B. Dollet, V. Leroy, *Phys. Rev. Lett.*, 2014, **112**, 148307.
- [7] I. Cantat, S. Cohen-Addad, F. Elias, F. Graner, R. Hohler, O. Pitois, F. Rouyer, A. Saint-Jalmes, *Les mousses, Structure et dynamique*, Belin, 2010, English translation: ed. S. J. Cox, *Foams: Structure and Dynamics*, translated by R. Flatman, Oxford University Press, 2013
- [8] J. G. H. Joosten, *J. Chem. Phys.*, 1984, **80**, 2383.
- [9] P. Sens, C. Marques, J.-F. Joanny, *Langmuir*, 1993 **9**, 3212.
- [10] C.-Y. D. Lu, M. E. Cates, *Langmuir*, 1995 **11**, 4225.
- [11] V. O. Afenchenko, A. B. Ezersky, S. V. Kiyashko, M. I. Rabinovich, P. D. Weidman, *Phys. Fluids*, 1998, **10**, 390.
- [12] A. Boudaoud, Y. Couder, M. Ben Amar, *Phys. Rev. Lett.*, 1999, **82**, 3847.
- [13] W. Drenckhan, B. Dollet, S. Hutzler, F. Elias, *Phil. Mag. Lett.*, 2008, **88**, 669.
- [14] Y. Couder, J. M. Chomaz, M. Rabaud, *Physica D*, 1989 **37**, 384.
- [15] J. F. Vignola, J. A. Judge, J. Jarzynski, M. Zalalutdinov, B. H. Houston, J. W. Baldwin, *Appl. Phys. Lett.*, 2006 **88**, 041921.
- [16] L. Bergmann, *J. Acoust. Soc. Am.*, 1956, **28**, 1043.
- [17] E. H. Lucassen-Reynders, J. Lucassen, *Adv. in Coll. Interf. Sci.*, 1969, **2**, 347.
- [18] C. Stenvot, D. Langevin, *Langmuir*, 1988, **4**, 1179.
- [19] I. Cantat, *Phys. Fluids*, 2013, **25**, 031303.